34th Annual International Conference of the IEEE EMBS
San Diego, California USA, 28 August - 1 September, 2012

Determining the Electrical Impedance of the Retina from a Complex Voltage Map

Nicholas A. Venables[1,2], Bahman Tahayori[1,2,*], *Member, IEEE*, Hamish Meffin[1,2,4], David B. Grayden[1,2,3,4], *Member, IEEE*, Anthony N. Burkitt[1,2,3,4], *Senior Member, IEEE*

***Abstract*— A method for determining the electrical impedance of the retina from complex valued voltage measurements is described. This is an extension to our previous work which did not consider the permittivity of the retina, or an exploration of the number of voltage measurements required to form an adequate solution. The model considers inhomogeneity in permittivity and conductivity of the tissue in both the x and y directions. This framework is tested on noisy voltage data solved for a synthetic rectangular retinal section. A synthetic retinal section inclusive of fovea is also considered. Estimates of the conductivity and permittivity maps are solved for using finite element analysis for a range of down sampling factors and signal to noise ratios for the voltage data. This is done to assess the potential accuracy of this method in a physical experiment.**

I. INTRODUCTION

A visual neuro-prosthesis can be used to restore the vision of a person suffering from a retinal degenerative disease [1]. The restoration of vision for such a patient is possible due to the generation of a spot of light, known as a phosphene, when the retina is electrically stimulated [2]. Many of these spots of light can be generated and controlled to give a light spot representation of the true surrounds.

The development of an optimal stimulation strategy is required to successfully develop a high-acuity device. This requires careful consideration of the geometry, penetration depth and pitch factor of the stimulating electrodes. Knowing the electrical impedance of the retina's layers accurately may assist in giving a more desirable and more timely solution to these questions. The difficulty in obtaining accurate measurements for the electrical impedance of a retina is due to the anisotropy and inhomogeneity of the tissue [3]. Resistivity depth profiles have been generated for a variety of mammal retinas including those of the rabbit, macaque and cat [4] [5] [6]. The results from Karwoski's paper [4] on calculating the resistivity profile of rabbit retinas suggest that the resistivity depth profiles of two retinas obtained from different animals of the same species may differ by at least 50%. Despite this, it is still desirable to establish some standard values for how the impedance varies throughout a human retina.

[1]NeuroEngineering Laboratory, Department of Electrical and Electronic Engineering, The University of Melbourne, Parkville, VIC 3010, Australia. [2]Centre for Neural Engineering, The University of Melbourne, Parkville, VIC 3010, Australia. [3]Bionics Institute 384-388 Albert Street, East Melbourne, VIC 3002. [4]NICTA Victoria Research Labs, The University of Melbourne, Parkville, VIC, 3010, Australia. *Corresponding author, bahmant@unimelb.edu.au.

When solving the resistivity profiles of different retinas, the assumption is that the retina is inhomogeneous in only one direction, through the retinal layers. It is also frequently assumed that the retina is homogeneous throughout each layer. This means that only a single value of resistivity is required to describe the entire layer's resistance. The accuracy of such an approach could be sufficient if the width of the layers was consistent across the length of the retina at all points. However, by viewing an image of the human retina obtained through Optical Coherence Tomography (OCT), it can be observed that this is not the case [7]. In the region of tissue surrounding the fovea, the retinal layer structure breaks down and the layers are indistinguishable from one another [8]. For a retinal prosthesis, even if the site of retinal stimulation was not located at the fovea, the electrical impedance of the retina in that area could affect the charge density at the site of stimulation. For this reason, we have developed a method to determine the electrical impedance of the regions surrounding the fovea.

A variety of resistivity profiles of the retina have been calculated [9], but no method to determine the permittivity profile of the retina exists to our knowledge. Complex voltage measurements can be taken when a sinusoidal voltage is applied to the retina section. The complex impedance of the retina can then be determined from this data. Here, we detail a method of determining the electrical impedance of the retina, which is an extension to our previous work which did not consider permittivity [10].

The rest of the paper is structured as follows. In Section II, the theory for the *forward* and *backward problems* is presented. Section III presents Finite Element Method (FEM) simulation results for two different hypothetical retinal sections. Discussion of these results is detailed in Section IV.

II. METHODS

The retinal section can be modeled as being contained in a simply connected set Ω defined in two-dimensional Euclidian space, $\mathbb{R}^2$. The approach presented here models inhomogeneity in the conductivity, σ, and the relative permittivity, ϵ_r, in both the x and y directions. For such a surface with suitably defined boundary conditions and an Alternating Current (AC) voltage V_{ac} of radial frequency ω, as shown in Figure 1, the equation in steady state is given by

$$\nabla \cdot ((\sigma(x,y) + j\omega\epsilon_0\epsilon_r(x,y))\nabla v(x,y)) = 0, \qquad (1)$$

where $x, y \in \mathbb{R}$. An assessment must be made of the effectiveness of our established method to illustrate the

potential accuracy of our approach. To this end, hypothetical $\sigma(x, y)$ and $\epsilon_r(x, y)$ data for a two-dimensional geometry representing the retina is created. It is worth noting that, in practice, $\sigma(x, y)$ and $\epsilon_r(x, y)$ are also dependent on ω; however, for this proof of principle procedure, this has no bearing on the problem formulation. A complex valued voltage map, $v(x, y)$, can then be determined for a given applied sinusoidal voltage of radial frequency, ω. Estimations of the conductivity and permittivity maps, denoted by $\hat{\sigma}(x, y)$ and $\hat{\epsilon}_r(x, y)$, respectively, are computed. The process of determining the voltage map, $v(x, y)$, is referred to as the *forward problem* while using that map to solve for $\hat{\sigma}(x, y)$ and $\hat{\epsilon}_r(x, y)$ is named the *backward problem*. In an experimental setting, only the *backward problem* requires solution, as $v(x, y)$ is obtained through measurement. Once conductivity and permittivity maps have been calculated, a direct comparison can be made between the estimated values, $\hat{\sigma}(x, y)$ and $\hat{\epsilon}_r(x, y)$, with the true values, $\sigma(x, y)$ and $\epsilon_r(x, y)$. The smaller the difference between the estimated and original maps, the more likely that this method would yield an accurate result in practice.

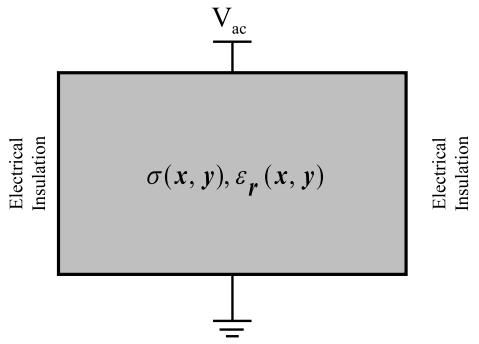

Fig. 1. The experimental setup for the forward problem where the tissue has one side set to V_{ac}, one side set to ground and two insulated sides.

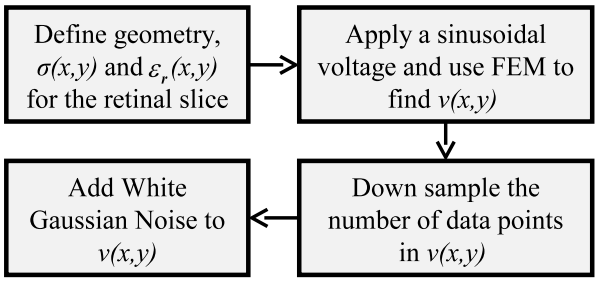

Fig. 2. The steps required for solving the *forward problem*.

Any voltage measurement taken has some level of inherent noise present in the signal. For this reason, white Gaussian noise has been added to $v(x, y)$ to make our solution have more relevance to the actual experimental case. In practice, there will be constraints on the number of voltage measurements that can be taken of the tissue, as the tissue will deform with each successive electrode penetration. While multiple measurements at the one location could be taken of the

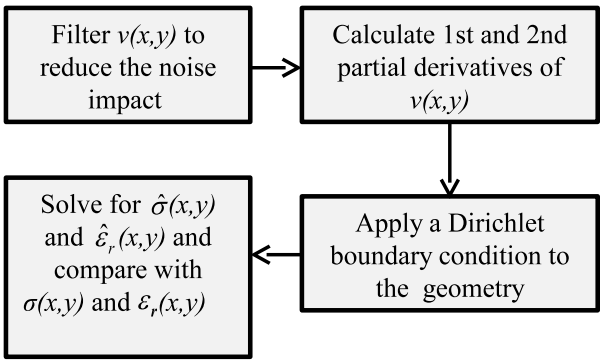

Fig. 3. The steps required for solving the *backward problem*.

voltage, there will be limitations on the number of locations at which measurements can be taken. To consider this in our model, a grid with a variable spacing between voltage measurements is sampled from $v(x, y)$ prior to solution of the *backward problem*. The steps for solving the *forward problem* are shown in Figure 2 and those for solving the *backward problem* are shown in Figure 3.

A. Forward Problem Methodology

The intention of the *forward problem* is to establish the complex valued voltage map, $v(x, y)$, generated when an AC voltage source is applied across the tissue as shown in Figure 1. Equation (1) can be expanded in Cartesian coordinates to give

$$\left(\sigma(x,y)+j\omega\epsilon_0\epsilon_r(x,y)\right)\left(\frac{\partial^2 v}{\partial x^2}+\frac{\partial^2 v}{\partial y^2}\right)+\frac{\partial\sigma(x,y)}{\partial x}\frac{\partial v}{\partial x} +\frac{\partial\sigma(x,y)}{\partial y}\frac{\partial v}{\partial y}+j\omega\epsilon_0\left(\frac{\partial\epsilon_r(x,y)}{\partial x}\frac{\partial v}{\partial x}+\frac{\partial\epsilon_r(x,y)}{\partial y}\frac{\partial v}{\partial y}\right)=0, \tag{2}$$

with the boundary conditions

$$v(y=y_0)=0,\quad v(y=y_1)=V_{ac},\quad \frac{\partial v}{\partial x}\Big|_{x=x_0}=0,\quad \frac{\partial v}{\partial x}\Big|_{x=x_1}=0. \tag{3}$$

Equation (2), which is a second order linear Partial Differential Equation (PDE) in terms of the dependent variable v, is solved to find the voltage map on the tissue.

B. Backward Problem Methodology

In the *backward problem*, the conductivity and permittivity maps are not known and are estimated from the complex voltage map generated in the solution to the *forward problem*, along with a suitable Dirichlet boundary conditions. Equation (2) can be used to find an estimate of $\hat{\sigma}(x, y)$ and $\hat{\epsilon}(x, y)$ as the dependent variables.

C. Simulation Methodology

The solutions of the *forward* and *backward problems* were obtained using COMSOL 4.2a, a finite element analysis package. MATLAB 2010a was used to down-sample the voltage map, $v(x, y)$. MATLAB was then used to add white

Gaussian noise, perform filtering routines and take derivatives. The voltage map was then exported to COMSOL and interpolated to form coefficients of Equation (2) to solve for the dependent variables, $\sigma(x,y)$ and $\epsilon(x,y)$. The *Electric Currents* module in COMSOL in *Frequency Domain* mode was used for solving the *forward problem*. The *Coefficient Form PDE (c)* model in the *Mathematics* module was employed to solve the *backward problem*. COMSOL was used to define the retinal geometry as well as its conductivity and permittivity maps. The solver, *Direct PARDISO* with its default parameters was used for the final solution of the *forward* and *backward problems*.

III. SIMULATION RESULTS

To illustrate the potential effectiveness of the method, the simulations presented here are for an inhomogeneous layer and a fovea conductivity map in a solution.

A. Example 1: Inhomogeneous Layer

The first example is a single inhomogeneous layer where the conductivity and permittivity vary in both the x and y directions. We consider a conductivity map of form

$$\sigma(x,y)=1+0.2\Big(\sin\frac{x}{50\times10^{-6}}\Big)+0.3\Big(\cos\frac{y}{40\times10^{-6}}\Big), \tag{4}$$

as shown in Figure 4, and a permittivity map of form

$$\epsilon(x,y)=90+10\Big(\cos\frac{x}{30\times10^{-6}}\Big)+5\Big(\sin\frac{y}{25\times10^{-6}}\Big), \tag{5}$$

as shown in Figure 5.

Using the procedure described in Section II we calculated estimates for the conductivity and permittivity maps of the layer described by Equations (4) and (5).

The error maps between $\sigma(x,y)$ and $\hat{\sigma}(x,y)$ as well as $\epsilon(x,y)$ and $\hat{\epsilon}(x,y)$ are shown in Figure 6 and Figure 7, respectively. The impact that the noise level in $v(x,y)$ has on the error is shown in Figure 8 while Figure 9 indicates how the number of measurements used to formulate a solution affects the error.

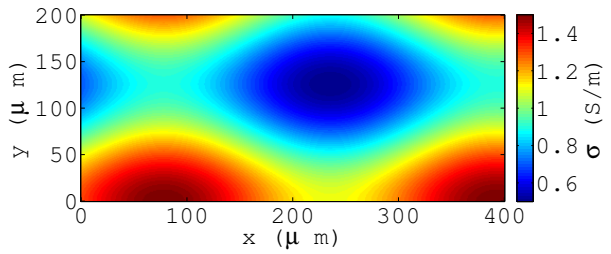

Fig. 4. The synthetic conductivity map described by Equation (4) applied to a 400μm×200μm geometry.

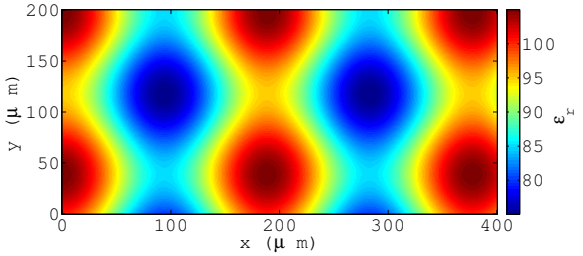

Fig. 5. The synthetic permittivity map described by Equation (5) applied to a 400μm×200μm geometry.

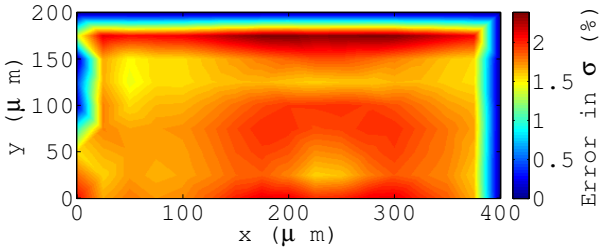

Fig. 6. The percentage error at each point between $\sigma(x,y)$ and $\hat{\sigma}(x,y)$.

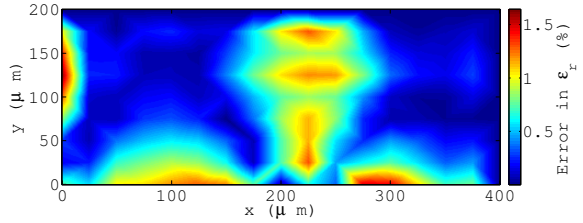

Fig. 7. The percentage error at each point between $\epsilon(x,y)$ and $\hat{\epsilon}(x,y)$.

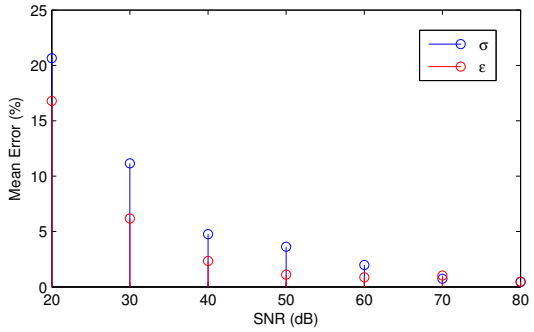

Fig. 8. The mean percentage error between the $\sigma(x,y)$ and $\hat{\sigma}(x,y)$ and the $\epsilon(x,y)$ and $\hat{\epsilon}(x,y)$ maps for a range of SNRs and a 5 μm spacing of measurements.

B. Example 2: Fovea

Estimates are made for a simple three layer fovea model. The result shown here is only for the $\sigma(x,y)$ map for the sake of brevity. The fovea is modeled as being suspended in a saline solution of $\sigma = 2$S/m. This is done to provide suitable boundary conditions for the problem. The $\sigma(x,y)$ map defined for the multi layer fovea is presented in Figure 10. The resulting error map after solving the *foward* and *backward problems* between $\sigma(x,y)$ and $\hat{\sigma}(x,y)$ is represented in Figure 11.

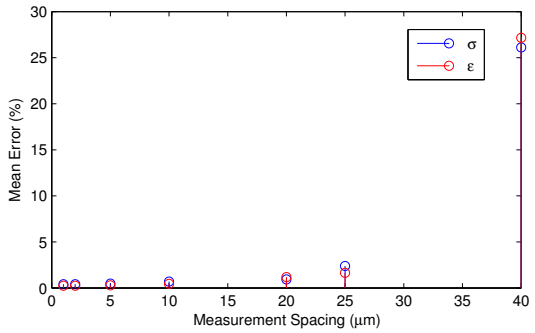

Fig. 9. The mean percentage error between the $\sigma(x, y)$ and $\hat{\sigma}(x, y)$ and the $\epsilon(x, y)$ and $\hat{\epsilon}(x, y)$ maps for a range of measurement spacing.

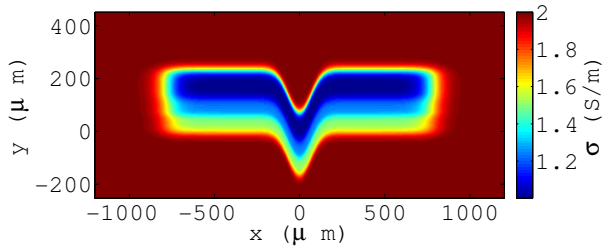

Fig. 10. The conductivity map of a three layer fovea with layers of, $\sigma_1 = 1$S/m, $\sigma_2 = 1.25$S/m and $\sigma_3 = 1.5$S/m. The fovea, approximated as a Gaussian function in a saline solution of $\sigma_s = 2$S/m.

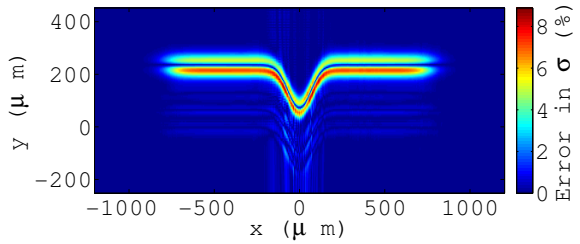

Fig. 11. The percentage error map between $\sigma(x, y)$ and $\hat{\sigma}(x, y)$.

IV. DISCUSSION AND CONCLUSIONS

The proposed method could yield conductivity and permittivity maps for the retina with potentially suitable accuracy. However, there are some issues that must be resolved to optimise our proposed method. The results determined through this method are dependent on the first and second partial derivatives of the complex voltage map $v(x, y)$. Due to the amplification of noise during the taking of derivatives, an optimal filter must be determined for the removal of the noise present in $v(x, y)$. In order to do this, a better understanding of the noise distribution to be encountered in such an experiment is required. The accuracy of the approach is highly dependent on the true frequency content of the spatially varying conductivity and permittivity of the retina. The Nyquist sampling criteria suggests we must take voltage measurements at a minimum rate of twice the highest frequency present in the voltage map. It is not possible to know the true frequency content of the signal without being alerted when sufficient voltage measurements have been taken. One solution may be to use a smaller voltage measurements spacing near the boundaries between layers which can be observed through an assessment of OCT data. Exact knowledge of the conductivity and the permittivity at the boundaries of the experimental area are required to obtain an accurate answer. This requires the retinal slice to be placed in a solution of known conductivity and permittivity. While this is achievable, much care is to be taken in the selection of an appropriate solution. If the difference in σ and ϵ for the tissue compared with that of σ and ϵ for the solution, the number of voltage samples required to obtain a sufficiently accurate solution may be far too large to be practically achievable. This method could, in theory, be used to determine the conductivity and the permittivity of the tissue for a range of frequencies by varying the frequency of the voltage source, V_{ac}. However, despite the possibility of this method yielding a desirable result in practice, the experiment would not be without its challenges and unknowns.

V. ACKNOWLEDGMENTS

This research was supported by the Australian Research Council (ARC) through its Special Research Initiative (SRI) in Bionic Vision Science and Technology grant to Bionic Vision Australia (BVA). The Bionics Institute acknowledges the support it receives from the Victorian Government through its Operational Infrastructure Support Program.

REFERENCES

[1] D. Palanker, A. Vankov, P. Huie, and S. Baccus, "Design of a high-resolution optoelectronic retinal prosthesis," *Journal of Neural Engineering*, vol. 2, no. 1, p. S105, 2005.

[2] J. ao C. Martins and L. Sousa, *Bioelectronic Vision: Retina Models, Evaluation Metrics and System Design*. Bioengineering & Biomedical Engineering Series, Vol.3, World Scientific, January 2009.

[3] C. J. Karwoski, D. A. Frambach, and L. M. Proenza, "Laminar profile of resistivity in frog retina." *J Neurophysiology*, vol. 54, no. 6, pp. 1607–19, 1985.

[4] C. Karwoski and X. Xu, "Current-source density analysis of light evoked field potentials in rabbit retina," *Visual Neuroscience*, vol. 16, pp. 369–377, 1999.

[5] H. Heynen and D. Norren, "Origin of the electroretinogram in the intact macaque eye–ii. current source-density analysis," *Vision Res.*, vol. 25, no. 5, pp. 709–715, 1985.

[6] U. Mitzdorf and W. Singer, "Prominent excitatory pathways in the cat visual cortex (a17 and a18): a current source density analysis of electrically evoked potentials," *Experimental Brain Research*, vol. 33, pp. 371–394, 1978.

[7] H. Chung, E. Kim, S. Kim, S. Park, J. Seo, and S. Woo, "A suprachoroidal electrical retinal stimulator design for long-term animal experiments and in vivo assessment of its feasibility and biocompatibility in rabbits," *Journal of Biomedicine and Biotechnology*, vol. 2008, p. 9, 2008.

[8] J. Wang, R. Spencer, J. Leffler, and E. Birch, "Critical period for the foveal fine structure in children with regressed retinopathy of prematurity," in *The American Association for Pediatric Ophthalmology and Strabismus annual meeting*, 2010, p. 3.

[9] C. J. Karwoski, X. Xu, and H. Yu, "Current-source density analysis of the electroretinogram of the frog: methodological issues and origin of components," *J. Opt. Soc. Am. A*, vol. 13, no. 3, pp. 549–556, Mar 1996.

[10] B. Tahayori, H. Meffin, N. Venables, D. Grayden, and A. Burkitt, "Theoretical framework for estimating the conductivity map of the retina through finite element analysis," in *Proceedings of the 33rd IEEE Conference on Engineering in Medicine and Biology*, 2011, pp. 6721–6724.